Chapter 2

From Visual Guidance in Flying Insects to Autonomous Aerial Vehicles

Mandyam V. Srinivasan, Saul Thurrowgood, and Dean Soccol

Abstract Investigation of the principles of visually guided flight in insects is offering novel, computationally elegant solutions to challenges in machine vision and robot navigation. Insects perform remarkably well at seeing and perceiving the world and navigating effectively in it, despite possessing a brain that weighs less than a milligram and carries fewer than 0.01% as many neurons as ours does. Although most insects lack stereovision, they use a number of ingenious strategies for perceiving their world in three dimensions and navigating successfully in it. Over the past 20 years, research in our laboratory and elsewhere is revealing that flying insects rely primarily on cues derived from image motion ("optic flow") to distinguish objects from backgrounds, to negotiate narrow gaps, to regulate flight speed, to compensate for headwinds and crosswinds, to estimate distance flown and to orchestrate smooth landings. Here we summarize some of these findings and describe a vision system currently being designed to facilitate automated terrain following and landing.

2.1 Introduction

Insect eyes differ from vertebrate or human eyes in a number of ways. Unlike vertebrates, insects have immobile eyes with fixed-focus optics. Therefore, they cannot infer the distances to objects or surfaces from the extent to which the directions of gaze must converge to view the object, or by monitoring the refractive power that is required to bring the image of the object into focus on the retina. Furthermore, compared with human eyes, the eyes of insects are positioned much closer together and possess inferior spatial acuity [16]. Therefore, the precision with which insects could estimate range through binocular stereopsis would be much poorer and restricted to relatively small distances, even if they possessed the requisite neural apparatus [15]. Not surprisingly, then, insects have evolved alternative strategies for dealing with the problems of visually guided flight. Many of these strategies rely on using image motion, generated by the insect's own motion, to infer the distances to obstacles and to control various manoeuvres (Franceschini, Chap. 3 of this volume) [10, 16, 21, 22].

This pattern of image motion, known as "optic flow", is used in many ways to guide flight. For example, distances to objects are gauged in terms of the apparent speeds of motion of the objects' images, rather than by using complex stereo mechanisms [12, 17, 26]. Objects are distinguished from backgrounds by sensing the apparent relative motion at the boundary [18]. Narrow gaps are negotiated safely by balancing the apparent speeds of the images in the two eyes [11, 19]. The speed of flight is regulated by holding constant the average image velocity as seen by both eyes [1, 5, 27]. This ensures that flight speed is automatically lowered in cluttered environments and that thrust is appropriately adjusted to compensate for headwinds and tail winds [2, 27]. Visual cues are also used to compensate for crosswinds. Bees landing on a horizontal surface hold constant the image velocity of the surface

M.V. Srinivasan (✉)
Queensland Brain Institute and ARC Centre of Excellence in Vision Science, University of Queensland, St. Lucia, QLD 4072, Australia
e-mail: M.Srinivasan@uq.edu.au

as they approach it, thus automatically ensuring that flight speed is close to zero at touchdown [24]. Foraging bees gauge distance flown by integrating optic flow: they possess a visually driven "odometer" that is robust to variations in wind, body weight, energy expenditure and the properties of the visual environment [4, 6, 7, 23].

In this chapter we concentrate on two aspects of visually guided navigation in flying insects, which are heavily reliant on optic flow. One relates to landing on a horizontal surface. The other concerns a related behaviour, terrain following, which involves maintaining a constant height above the ground and following the local fluctuations of terrain altitude.

2.2　Landing on a Horizontal Surface

We begin by summarizing the results of experiments that were conducted a few years ago in our laboratory to elucidate the visual mechanisms that guide landing in honeybees. How does a bee land on a horizontal surface? When an insect makes a grazing landing on a flat surface, the dominant pattern of image motion generated by the surface is a translatory flow in the front-to-back direction. What are the processes by which such landings are orchestrated?

Srinivasan et al. [24] investigated this question by video-filming trajectories, in three dimensions, of bees landing on a flat, horizontal surface. Two examples of landing trajectories, reconstructed from the data, are shown in Fig. 2.1a,b. A number of such landings were analysed to examine the variation of the instantaneous height above the surface (h), instantaneous horizontal (forward) flight speed (V_f), instantaneous descent speed (V_d) and descent angle (α). These variables are illustrated in Fig. 2.1c. Analysis of the landing trajectories revealed that the descent angles were indeed quite shallow. The average value measured in 26 trajectories was ca. 28° [24].

Figure 2.2a,b shows the variation of flight speed with height above the surface, analysed for two landing trajectories. These data reveal one of the most striking and consistent observations of this study: Horizontal speed is roughly proportional to height, as indicated by the linear regression on the data. When a bee flies at a horizontal speed of V_f (cm/s) at a height of h (cm), the angular velocity ω of the image of the surface directly

beneath the eye is given by

$$\omega = \frac{V_f}{h} rad/s \qquad (2.1)$$

From this relationship it is clear that, if the bee's horizontal flight speed is proportional to her height above the surface (as shown by the data), then the angular velocity of the image of the surface, as seen by the eye, must be constant as the bee approaches it. This angular velocity is given by the slope of the regression line. The angular velocity of the image varies from one trajectory to another, but is maintained at an approximately constant value in any given landing. An analysis of 26 landing trajectories revealed a mean image angular velocity of ca. 500°/s [24].

These results reveal two important characteristics. First, bees landing on a horizontal surface tend to approach the surface at a relatively shallow descent angle. Second, landing bees tend to hold the angular velocity of the image of the ground constant as they approach it.

What is the significance of holding the angular velocity of the image of the ground constant during landing? One important consequence is that the horizontal speed of flight is then automatically reduced as the height decreases. In fact, by holding the image velocity constant, the horizontal speed is regulated to be proportional to the height above the ground, so that when the bee finally touches down (at zero height), her horizontal speed is zero, thus ensuring a smooth landing. The attractive feature of this simple strategy is that it does not require explicit measurement or knowledge of the speed of flight or the height above the ground. Thus, stereoscopic methods of measuring the distance of the surface (which many insects probably do not possess) are not required. What is required, however, is that the insect be constantly in motion, because the image motion resulting from the insect's own motion is crucial in controlling the landing.

The above strategy ensures that the bee's horizontal speed is zero at touchdown, but does not regulate the descent speed. How does the descent speed vary during the landing process? Plots of descent speed versus height reveal a linear relationship between these two variables, as well. Two examples are shown in Fig. 2.2c,d. This finding implies that landing bees (i) adjust their forward (i.e. flight) speed to hold the
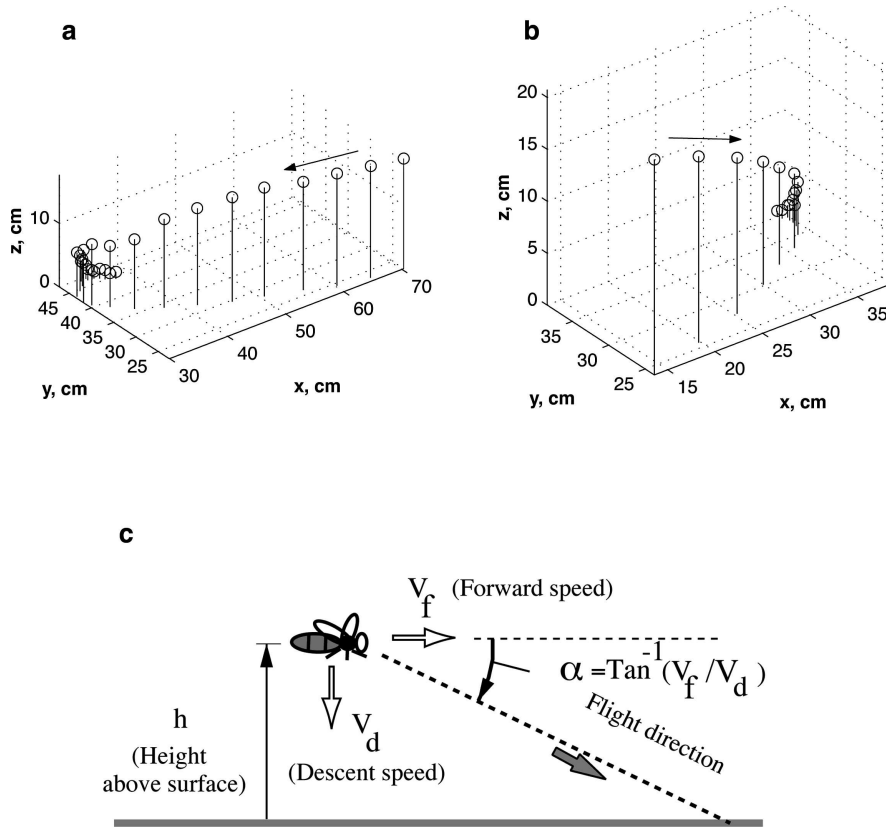
Fig. 2.1 (**a, b**) Three-dimensional reconstruction of two typical landing trajectories, from video films. *Vertical lines* depict the height above surface. (**c**) Illustration of some of the variables analysed to investigate the control of landing. *h* (cm): height above surface; V_f (cm/s): horizontal (forward) flight speed; V_d (cm/s): vertical (descent) speed; α (deg or rad): descent angle [$\alpha = (\tan^{-1}(V_f/V_d))$]. Adapted from [24]

image velocity of the ground constant and (ii) couple the descent speed to the forward speed, so that the descent speed decreases with the forward speed and also becomes zero at touchdown.

These results reveal what appears to be a surprisingly simple and effective strategy for making grazing landings on flat surfaces. A safe, smooth landing is ensured by following two simple rules: (a) adjusting the speed of forward flight to hold constant the angular velocity of the image of the surface as seen by the eye and (b) making the speed of descent proportional to the forward speed, i.e. flying at a constant descent angle. This produces landing trajectories in which the forward speed and the descent speed decrease progressively as the surface is approached, both approaching zero at touchdown.

What are the advantages, if any, of using this landing strategy? We can think of three attractive features. First, the strategy is very simple because it does not

require explicit knowledge of instantaneous height or flight speed. Second, forward and descent speeds are adjusted in such a way as to hold the image velocity *constant*. This is advantageous because the image velocity can then be maintained at a level at which the visual system is most sensitive to deviations from the "set" velocity, thereby ensuring that the control of flight is as precise as possible. An alternative strategy, for instance, might be to approach the surface at constant flight speed, decelerating only towards the end. Such a constant speed approach, however, would cause the image velocity to increase rapidly as the surface is approached and to reach levels at which the image velocity measurements may no longer be precise enough for adequate flight control. This situation would be avoided by the bee's landing strategy, which holds the image velocity constant. Third, an interesting by-product of the bee's landing strategy is that the projected time to touchdown is constant throughout the
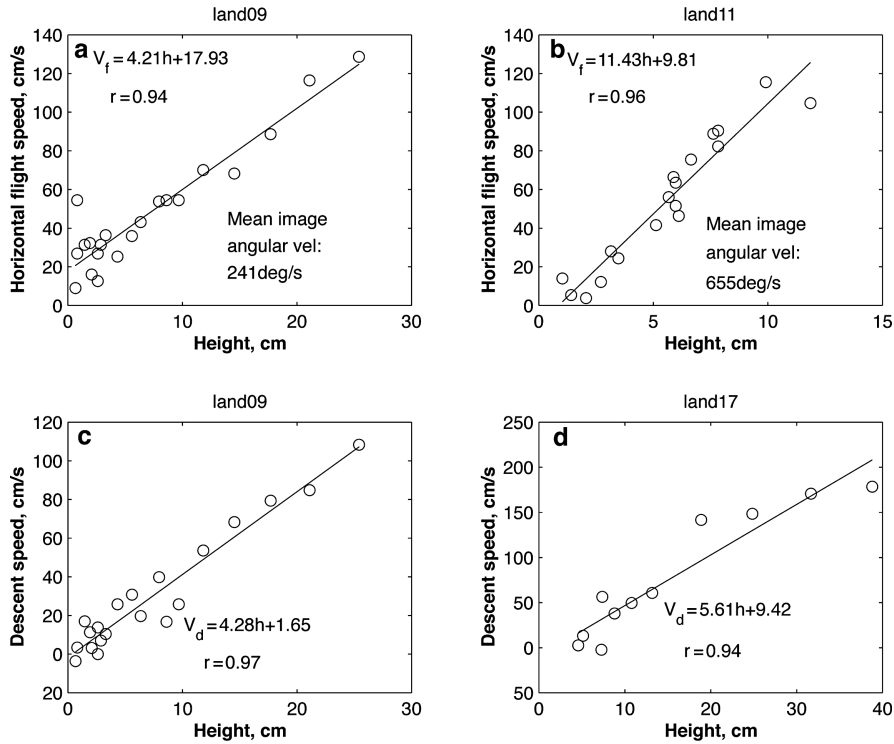
Fig. 2.2 (**a, b**) Variation of horizontal flight speed (V_f) with height (h) above the surface for two different landing trajectories. (**c, d**) Variation of descent speed (V_d) with height (h) above the surface for two different landing trajectories. The *straight lines* are linear regressions through the data, as represented by the equations; r denotes the regression coefficient. Adapted from [24]

landing process (details in [24]). In other words, if, at any time during the landing process, the bees were to stop decelerating and continue downward at constant velocity, the time to contact the ground would be the same, regardless of where this occurs in the landing trajectory. From the landing trajectories, one calculates a projected time to touchdown of about 0.22 s. Thus, it appears that landing bees allow themselves a "safety margin" of a fifth of a second to prepare for touchdown if they were to abandon the prescribed landing strategy at any point, for whatever reason, and proceed towards the ground in the same direction without further deceleration.

2.3 Terrain Following

A simple modification of the landing strategy described above can be used, in principle, to regulate the height above the ground during cruising flight. Here the aim is to maintain a constant height above the ground and to fly parallel to the surface by following any fluctuations of height (terrain following). The strategy would now be not to fly towards a target on the ground, but instead towards a distant target or the horizon. This will ensure a level flight attitude. Flight speed is held constant by maintaining a constant forward thrust (which should be effective, at least in still air). The height above the ground is regulated by adjusting the altitude so that the magnitude of the optic flow generated by the ground is constant. If the forward flight speed is V_f and the desired height above the ground is h, the magnitude of the optic flow that is to be maintained is given by Eq. (2.1) above as simply the ratio of V_f to h. If the measured optic flow is greater than this target value, it signifies that the altitude is lower than the desired value and a control command is then generated to increase altitude until the target magnitude of optic flow is attained. If the optic flow is lower than the target value, the opposite control command is issued, to again restore the optic flow to its desired level. This strategy has been tested successfully in simulations, in tethered robots in the laboratory and in some

freely flying model aircraft (Franceschini, Chap. 3 of this volume; Zufferey et al., Chap. 6 of this volume) [3, 13, 14, 25, 28].

2.4 Practical Problems with the Measurement of Optic Flow

When flying at low altitudes or during landing, the image of the ground can move very rapidly, making it difficult to obtain accurate estimates of optic flow. Here we describe a specially shaped mirror surface that, first, scales down the speed of image motion as seen by the camera and, second, removes the perspective distortion (and therefore the distortion in image velocity) that a camera experiences when viewing a horizontal plane that stretches out to infinity in front of the aircraft. Ideally, the moving image that is captured by the camera through the mirror should exhibit a constant, low velocity everywhere, thus simplifying the optic flow measurements and increasing their accuracy (see Fig. 2.3).
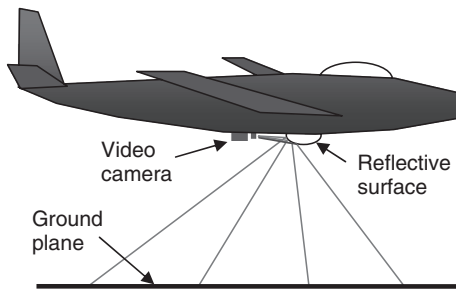

Fig. 2.3 Illustration of a system for visually guided terrain following and landing. The optical system is shown on an enlarged scale relative to the aircraft in order to illustrate its configuration

2.5 A Mirror-Based Vision System for Terrain Following and Landing

We seek a mirror profile that will map equal distances along the ground in the flight direction to equal displacements in the image plane of the camera. The geometry of the camera–mirror configuration is shown in Fig. 2.4. A′ is the camera image of a point A on the ground. We want A′ (the image of A) to move at a con-
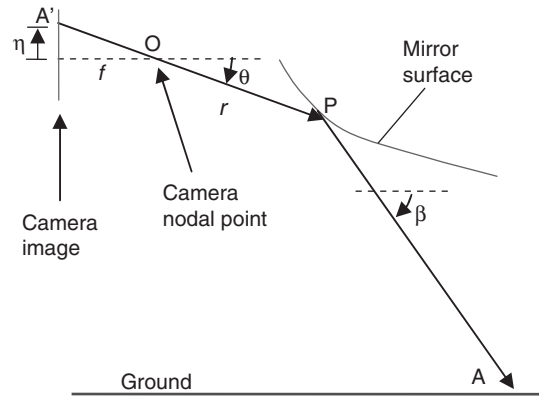

Fig. 2.4 Geometry of camera/mirror configuration for the design of mirror profile. Modified from [20]

stant velocity in the image plane of the camera, independent of the position of A in the ground plane. That is, we require $\frac{d\eta}{dt} = L$, where η is the distance of the point A′ from the centre of the camera's image plane, and L is the desired constant velocity; f is the focal length of the camera. The derivation of a mirror profile that meets these objectives is given in [20] and we shall not repeat it here. Instead, we use an example profile to illustrate the performance of the mirror.

Figure 2.5 shows one example of a profile of the reflective surface and includes the computed ray paths. In this example the camera faces forward, in the direction of flight. The nodal point of the camera is at (0.0). The image plane of the camera is to the left of this point and is not included in the figure, but its reflection about the nodal point (an equivalent representation) is depicted by the vertical line to the right of the nodal point. Parameters used in this design are as follows: $V = 1000.0$ cm/s; $h = 100.0$ cm; $r_0 = 10.0$ cm; $f = 3.5$ cm; $L = 2.0$ cm/s, where V is the speed of the aircraft, h is the height above the ground, L is the image velocity, f is the focal length of the camera and r_0 is the distance from the nodal point of the camera to the tip of the reflective surface. If the camera was looking directly downwards at the ground, the image velocity of the ground would have been 35 cm/s; with the mirror, the image velocity is reduced to 2.0 cm/s. Thus, the mirror scales down the image velocity by a factor of 17.5.

The curvature of the mirror is highest in the region that images the ground directly beneath the aircraft, because this is the region of the ground that moves at the highest angular velocity with respect to the camera,
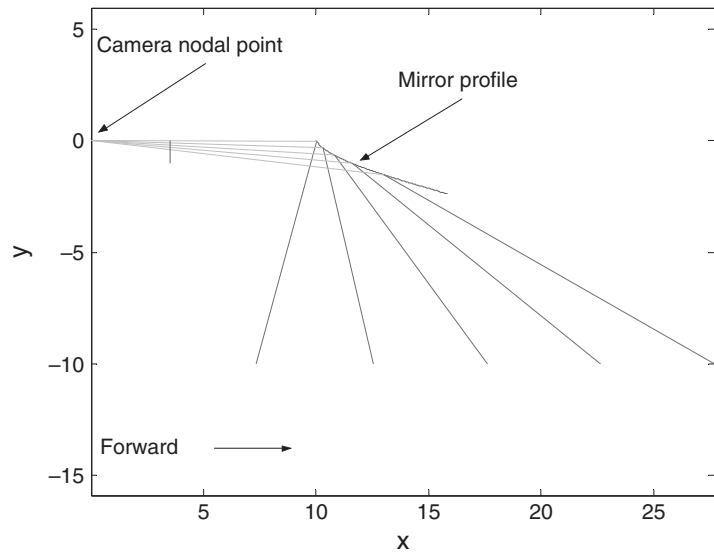
and which therefore requires the greatest reduction
of motion. We see from Fig. 2.5 that equally spaced
points on the ground along the line of flight map to
equally spaced points in the camera image. This con-
firms the correct operation of the surface.

Figure 2.6a illustrates the imaging properties of the
mirror, positioned with its axis parallel to and above a
plane carrying a checkerboard pattern. Note that the
mirror has removed the perspective distortion (fore-
shortening) of the image of the plane. The scale of the
mapping depends upon the radial direction. Compres-
sion is lowest in the vertical radial direction and high-
est in the horizontal radial direction.

Figure 2.6b shows a digitally remapped view of the
image in Fig. 2.6a, in which the polar co-ordinates of
each pixel in Fig. 2.6a are plotted as Cartesian co-
ordinates. Here the vertical axis represents radial dis-
tance from the centre of the image of Fig. 2.6a and the
horizontal axis represents the angle of rotation about

the optic axis. The circle in Fig. 2.6a maps to the hor-
izontal line in Fig. 2.6b. Regions below the line rep-
resent areas in front of the aircraft and regions above
it represent areas behind. Thus, the mirror endows the
camera with a large field of view that covers regions in
front of, below and behind the aircraft.

A consequence of the geometrical mapping pro-
duced by the mirror is that, for straight and level flight
parallel to the ground plane, the optic flow vectors will
have constant magnitude along each radius but will
be largest along the vertical radius and smallest (zero)
along the horizontal radius.

This is illustrated in Fig. 2.7, which shows the
optic flow vectors that are generated by a simulated
level flight over an ocean. Figure 2.7a shows the flow
field in the raw image and Fig. 2.7b the flow field
in the remapped image. In the remapped image, all
flow vectors are oriented vertically. The magnitudes
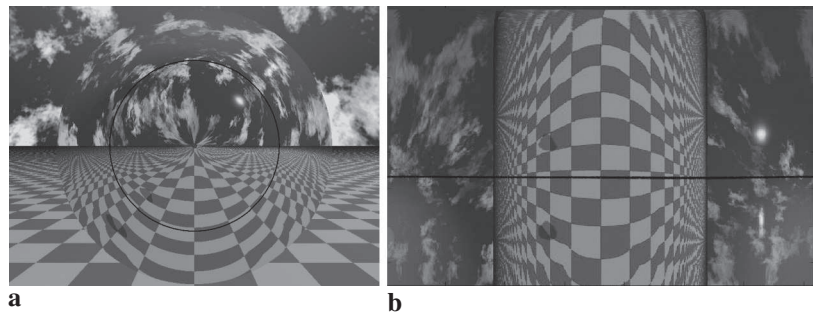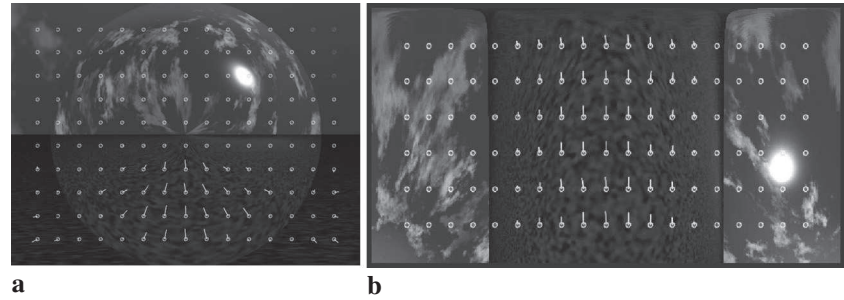of the vectors are constant within each column and

Fig. 2.6 (**a**) Illustration of
imaging properties of mirror
and (**b**) remapped version of
image in Fig. 2.6a. Adapted
from [20]

Fig. 2.7 Optic flow field
generated by simulated level
flight over an ocean. (**a**) The
flow in the raw image and
(**b**) the flow in the remapped
image. Adapted from [15]

decrease progressively with increasingly lateral directions of view. These vectors provide information on the height above the ground, the topography of the ground and the ranges to objects in the field of view (which is quite large).

If the system undergoes pure translation along its optic axis, as in Fig. 2.5, the magnitude of the optic flow vector at each point on the unwarped image will be inversely proportional to the distance of the viewed point from the optic axis of the system. Thus, the flow vectors will provide information on the profile of the terrain in a cylindrical co-ordinate system relative to the aircraft. The mapping that is provided by the mirror should be particularly useful for aircraft guidance. If a cylinder of "clear space" is desired for obstacle-free flight along a given trajectory, the maximum permissible flow magnitude is determined by the speed of the aircraft and the radius R of this cylinder (see Fig. 2.8). This simplifies the problem of determining in advance whether an intended flight trajectory through the environment will be collision-free and of making any necessary adjustments to the trajectory to ensure safe flight. The system will provide information on the height above the ground, as well as the distance of any potential obstacles, as measured from the optical axis.

2.6 Height Estimation and Obstacle Detection During Complex Motions

If the aircraft undergoes rotation as well as translation, the optic flow vectors that are induced by the rotational components of aircraft motion will contaminate the range measurement. They must be subtracted from the total optic flow field, to obtain a residual flow field that represents the optic flow that is created only by the translational component of aircraft motion. The rotations of the aircraft can be estimated through gyroscopic signals. Since each component of rotation (yaw, roll, pitch) produces a known, characteristic pattern of optic flow which depends on the magnitude of the rotation but is independent of the ranges of objects or surfaces in the environment, the optic flow vector fields that are generated by the rotations can be predicted computationally as a sum of the characteristic optic flow fields for yaw, pitch and roll, each weighted by the magnitude of the measured rotation about the corresponding axis. This composite rotational flow field must then be subtracted from the total flow field to obtain a residual flow field that represents the flow due to just the translational component of motion. The
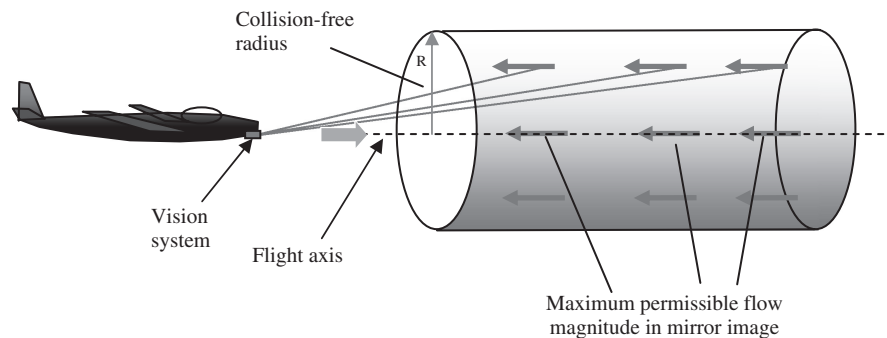

Fig. 2.8 Illustration of collision-free cylinder mapping achieved by the system. Modified from [15]

Collision-free radius

R

Vision system

Flight axis

Maximum permissible flow magnitude in mirror image

distances to objects and surfaces from the optical axis can then be computed from this residual field.

2.7 Hardware Realization and System Tests

The mirror profile shown in Fig. 2.5 was machined in aluminium on a numerically controlled lathe. It was mounted on a bracket, which also carried an analogue video CCD camera (320×240 pixels) with its optical axis aligned with the axis of the mirror. The nodal point of the camera's lens was positioned 10 cm from the tip of the mirror, as per the design specifications (see above).

In order to extract the range of objects during complex motions, it is necessary to first determine the flow signatures, or "templates", that characterise the patterns of optic flow during pure yaw, pure roll and pure pitch. This was done by using a robotic gantry to move the vision system in a richly textured visual environment. The environment consisted of a rectangular arena 3.05 m long, 2.2 m wide and 1.13 m tall (Fig. 2.9a). The walls and floor of the arena were lined with a texture composed of black circles of five different diameters (150 mm, 105 mm, 90 mm, 75 mm and 65 mm) on a white background. The rich visual texture permitted dense and accurate measurements of the optic flow in the lower hemisphere of the visual field.

A raw image of the arena, as acquired by the system, is shown in Fig. 2.10a. An unwarped version of this image is shown in Fig. 2.10b.

The gantry was used to position the optical axis of the system at a height of 650 cm above the floor. Optic flow templates for yaw, pitch and roll were obtained for the remapped images by using the gantry to rotate the vision system by small, known angles (ranging from 0.25° to 2.5°, in steps of 0.25°) about each of the three axes, in turn. Measurements were repeated with the vision system positioned at several different locations in the arena and the results were pooled and normalized to obtain reliable and dense estimates of the optic flow templates for a 1° rotation. (In theory, the rotational optic flow templates should be independent of the position or attitude of the vision system within the arena.) The optic flow was computed using a correlation algorithm [8]. The resulting rotational templates for yaw, roll and pitch are shown in Fig. 2.11, for rotations of 1° in each case.

For small angular rotations, the magnitude of the flow vector at any given point in the visual field should increase approximately linearly with the magnitude of the rotation, and the direction of the flow vector should remain approximately constant. This has been verified in [15]. Thus, we can legitimately scale the optic flow templates for the measured rotations in yaw, pitch and roll, in order to subtract out the contributions of each of these rotational components in a flow field that is generated by complex motion.

The next step was to test performance when the system executed compound motions that combined translation and rotation. The aim was to investigate whether the system could determine the range to objects in the environment (and specifically, the height above the ground) while executing complex motions. This investigation was performed by using the gantry to move the system along a trajectory along a curved trajectory, as shown in Fig. 2.9b.

Fig. 2.9 (**a**) View of vision system, carried by a robotic gantry in a visually textured arena and (**b**) plan view of a curved trajectory used to test the system. Adapted from [15]
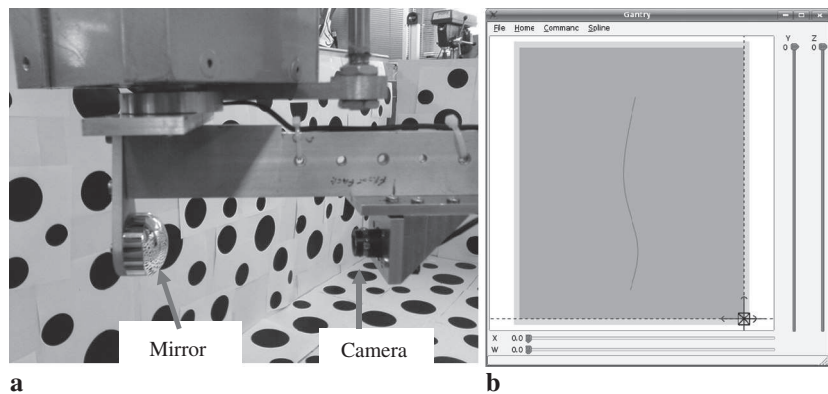
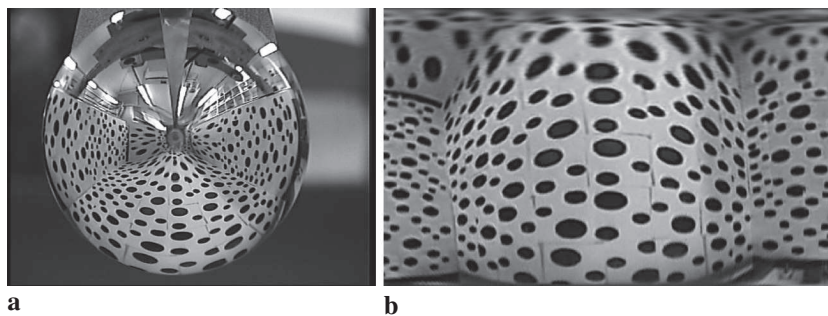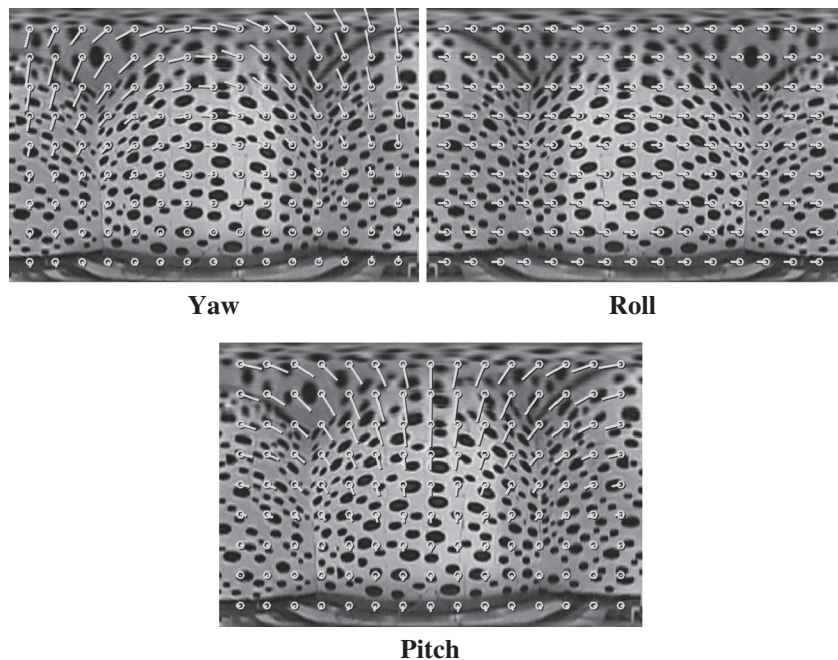**Fig. 2.10** Raw (**a**) and unwarped (**b**) images of the arena as viewed by the system. Adapted from [15]

a　　　　　　　　　　**b**

Fig. 2.11 Measured rotational templates for yaw, roll and pitch

Yaw　　　　　　　　　　**Roll**

Pitch

The height of the system was held constant at 650 mm above the floor throughout the trajectory. The trajectory consisted of a sequence of stepwise motions in the horizontal plane. The optical axis of the system was always aligned along the instantaneous direction of translation, i.e. it was parallel to the local tangent to the trajectory. Each step, in general, consisted of an elementary translation (of 50 mm) along the optical axis of the vision system, followed by an elementary yaw rotation of known, but variable, magnitude (ranging from $+2.9°$ to $-1.5°$). A visual frame was acquired from the camera at the end of each elementary step (translation or rotation).

Figure 2.12a shows the optic flow generated by a compound step, consisting of an elementary translation followed by an elementary rotation (yaw). This is the

flow that would be generated between two successive frames if the system had moved along a smooth curve.

Figure 2.12b shows the flow that would have been induced by the rotational component of motion that occurred during this compound step. This flow pattern was computed by weighting the template for yaw rotation by the (known) magnitude and polarity of the yaw that occurred during the compound step. (During flight, this yaw information would be obtained from a rate gyro.)

Figure 2.13a shows the optic flow that is obtained when the rotational component of the flow (from Fig. 2.12b) is subtracted from the total flow that is generated by the compound step (Fig. 2.12a). This residual flow should represent the flow that is induced solely by the translational component of the system's motion. It

Fig. 2.12 (**a**) Flow measured after a compound step consisting of translation followed by yaw and (**b**) flow induced by the rotational (yaw) component, calculated from the template for yaw. Adapted from [15]
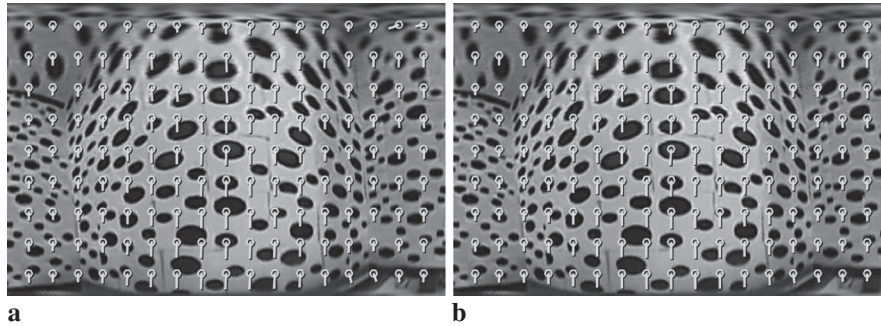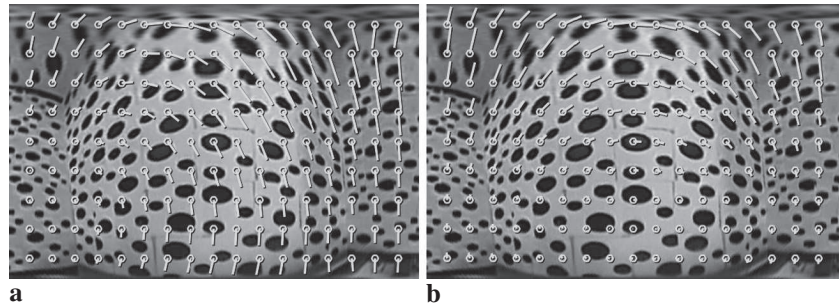

Fig. 2.13 (**a**) Residual flow obtained by subtracting the yaw-induced flow (Fig. 2.12b) from the measured flow (Fig. 2.12a). (**b**) Flow induced by the translatory component of motion in the compound step. Adapted from [15]

is evident that all the vectors in the residual flow field are parallel and vertical, as would be expected during pure translation. Furthermore, this pattern of optic flow is in excellent agreement with the pattern of flow that is actually generated by pure translation at this par-ticular location in the arena. This latter flow pattern, shown in Fig. 2.13b, is the flow measured between the two frames that bracketed the translatory segment of the compound step. A comparison of Fig. 2.13a,b reveals that these flow patterns are virtually identical.

Fig. 2.14 Results of extending the de-rotation procedure to roll as well as yaw. The figure shows one frame of a motion sequence in which the vision system executed a trajectory involving translation, yaw and roll. The *upper left panel* shows the raw image. The *upper right panel* shows one frame of the unwarped image and the instantaneous raw optic flow. The *lower right panel* shows the result of de-rotation, by using the roll and yaw templates to subtract the flow components induced by the measured roll and yaw
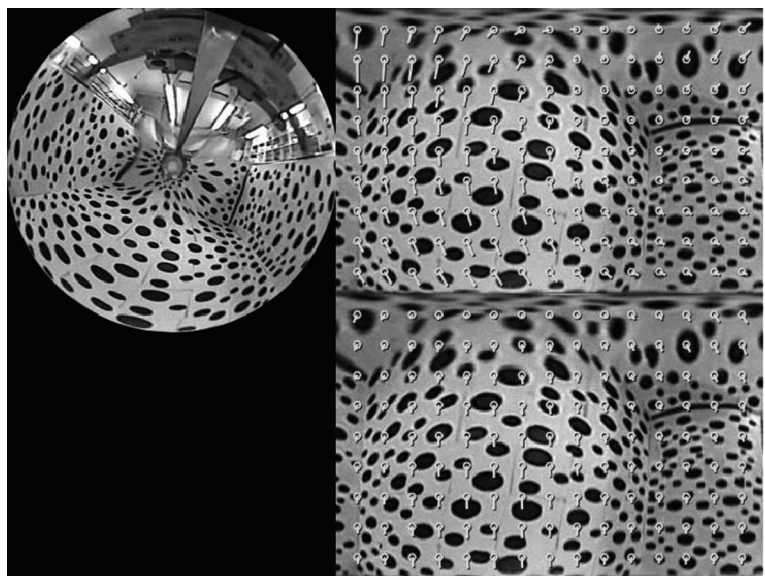
This result, which was obtained consistently for all the compound steps in the trajectory, demonstrates that the pattern of optic flow that is generated during a small but complex motion can be successfully "de-rotated" to extract the optic flow that is created purely by the translatory component of motion that occurred during the period.

The results of extending this de-rotation procedure to rotations about two axes – yaw and roll – are summarized in Fig. 2.14. Here again, after subtracting the optic flow components induced by yaw and roll, the residual optic flow is purely translatory, thus demonstrating the validity of the de-rotation procedure.

2.8 Extracting Information on Range and Topography

The final step is to examine whether the residual component of the optic flow (the translation-induced component) can be used to obtain accurate information on the range and profile of the terrain over which flight occurs. With reference to Figs. 2.7b and 2.13, for horizontal flight over level ground, the magnitudes of the translation-induced optic flow vectors should be a maximum in the central column (corresponding to the ground directly beneath the aircraft) and should fall off as a cosine function of the lateral angle of view (in the columns to the left and right; [20]). This should be true for any row of vectors.

This prediction is tested in Fig. 2.15a, which shows the variation of translatory flow magnitude with lateral angle for flow vectors in any given row, in data sets such as that shown in Fig. 2.13a. The results show the magnitude profiles for the vectors in the second row from the bottom, computed for each step of the trajectory. The second row represents a view that is oriented at approximately 90° to the axial direction (a lateral view). A least-squares analysis reveals that each of the profiles approximates a cosine function quite well. The thick red curve shows the mean of the cosine functions fitted to each of the profiles obtained along the trajectory. If the speed of the aircraft is known, the amplitude of this curve provides information on the height above the ground (the amplitude is inversely proportional to height). The mean amplitude of the curves is
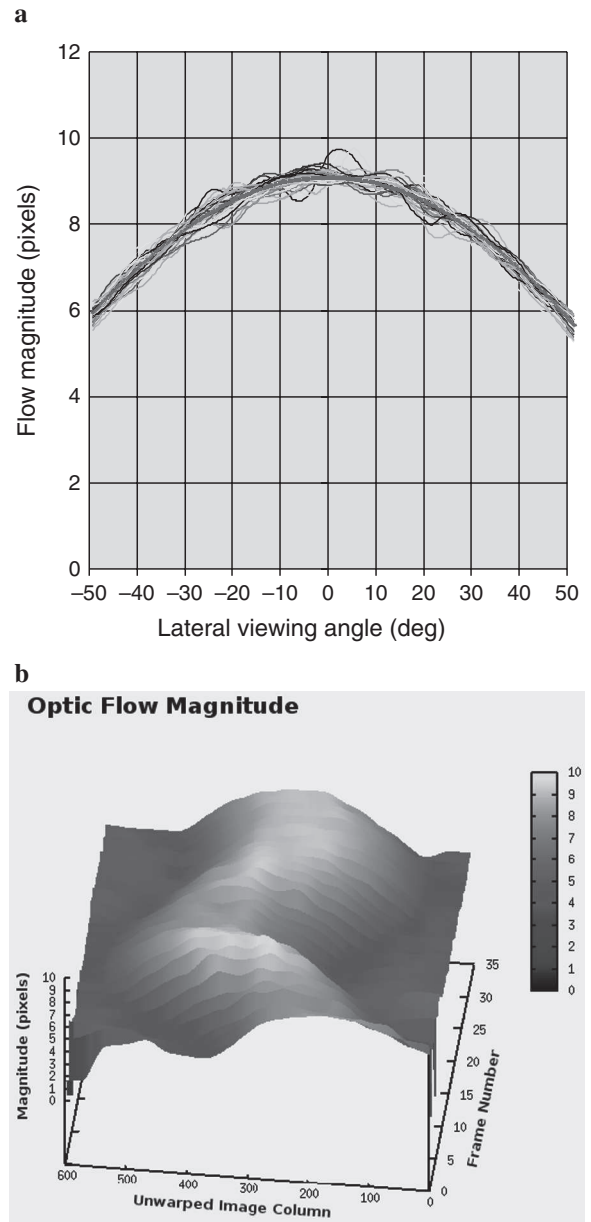

Fig. 2.15 (**a**) Variation of flow magnitude with lateral viewing angle in the residual flow field at each of the steps along the trajectory of Fig. 2.9b. Adapted from [15]. (**b**) Magnitudes of the de-rotated optic flow computed along the entire trajectory of a motion path involving translation and roll

9.076 pixels and the standard deviation is 0.062 pixels, indicating that the estimate of flight height is consistent and reliable throughout the trajectory of Fig. 2.9b.

Figure 2.15b shows the magnitudes of the de-rotated optic flow computed along the entire trajectory of a complex motion path involving translation and roll. It

is evident that, in each frame, the profile of the optic flow magnitude closely approximates a cosine function. The peak of the function wanders to the left or the right from frame to frame because the vision system is undergoing roll as well as translation, and the optic flow data are plotted in relation to the co-ordinates of the vision system.

2.9 Preliminary Flight Tests

Figure 2.16 shows a view of a prototype of the vision system mounted on the underside of a model aircraft. Figure 2.17 shows views of the raw camera image
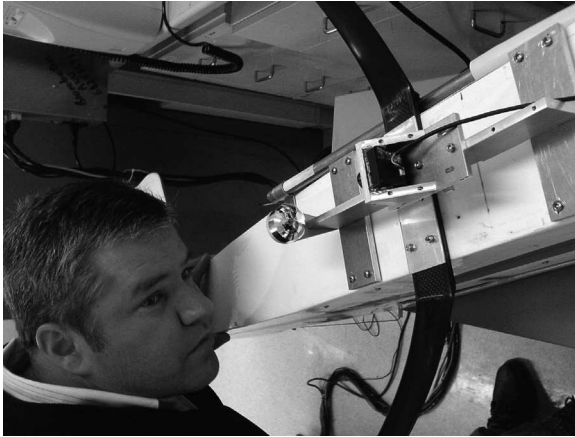
(left) and the unwarped image (right) with the computed optic flow vectors. The horizon (in the raw image as well as the unwarped image) distorts in predictable ways depending upon the roll and pitch attitudes of the aircraft. The horizon profile can thus be used to estimate the roll and pitch of the aircraft, when flying at high altitudes over reasonably flat terrain.

Figure 2.18a shows one frame of the unwarped camera image during a test flight, with the computed raw optic flow field. Figure 2.18b shows the same frame, with optic flow computed after de-rotation in yaw, pitch and roll, using information from the aircraft's gyroscopes. The optic flow vectors in the de-rotated field are all very close to vertical, indicating that the de-rotation procedure is successful and accurate.

2.10 Conclusions and Discussion

This study has described the design of a vision sensor, based partly on principles of insect vision and optic flow analysis, for the measurement and control of flight height and for obstacle avoidance. A video camera is used in conjunction with a specially shaped reflective surface to simplify the computation of optic flow and extend the range of aircraft speeds over which accurate data can be obtained. The imaging system also provides a useful geometrical remapping of the environment, which facilitates obstacle avoidance and
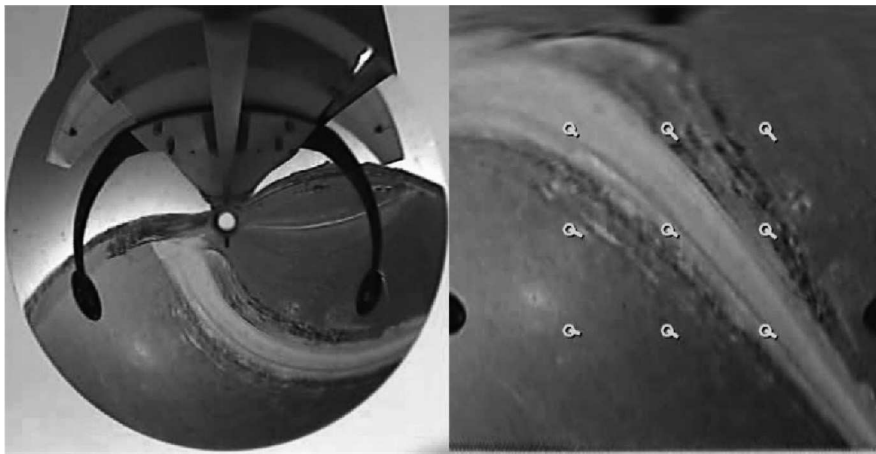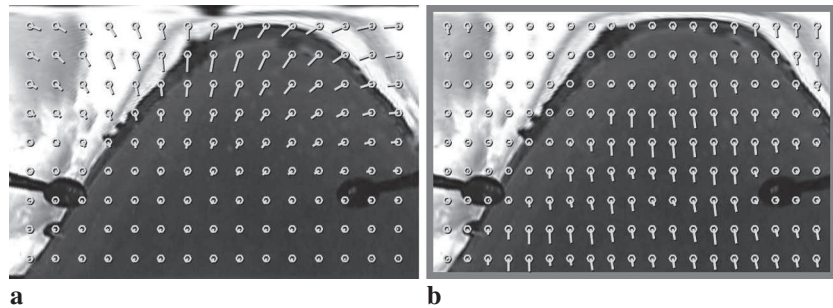

Fig. 2.16 View of vision system mounted on the underside of a model aircraft

Fig. 2.17 Test flight. Views of the raw camera image (*left*) and the unwarped image (*right*) with the computed optic flow vectors

Fig. 2.18 Test flight. (**a**) One frame of unwarped camera image, with computed raw optic flow field. (**b**) Same frame, with optic flow computed after de-rotation in yaw, pitch and roll

computation of three-dimensional terrain maps. By using calibrated optic flow templates for yaw, roll and pitch, accurate range information can be obtained even when the aircraft executes complex motions. In principle, the vision system described here can be used in the platforms described in (Franceschini, Chap. 3 of this volume Zufferey et al., Chap. 6 of this volume) to facilitate vision guidance during landing or when flying at high speeds close to obstacles or close to the ground. Future work with this system will involve open-loop and closed-loop tests on flying vehicles, to examine the utility of this approach for autonomous guidance.

References

1. Baird, E., Srinivasan, M.V., Zhang, S.W., Cowling, A.: Visual control of flight speed in honeybees. The Journal of Experimental Biology **208**, 3895–3905 (2005)
2. Barron, A., Srinivasan, M.V.: Visual regulation of ground speed and headwind compensation in freely flying honey bees (*Apis mellifera* L.). Journal of Experimental Biology **209**, 978–984 (2006)
3. Barrows, G.L., Chahl, J.S., Srinivasan, M.V.: Biologically inspired visual sensing and flight control. The Aeronautical Journal, London: The Royal Aeronautical Society **107**(1069), 159–168 (2003)
4. Dacke, M., Srinivasan, M.V.: Honeybee navigation: Distance estimation in the third dimension. Journal of Experimental Biology **210**, 845–853 (2007)
5. David, C.T.: Compensation for height in the control of groundspeed by *Drosophila* in a new, "Barber's Pole" wind tunnel. Journal of Comparative Physiology **147**, 485–493 (1982)
6. Esch, H., Burns, J.E.: Honeybees use optic flow to measure the distance of a food source. Naturwissenschaften **82**, 38–40 (1995)
7. Esch, H., Zhang, S.W., Srinivasan, M.V., Tautz, J.: Honeybee dances communicate distances measured by optic flow. Nature (London) **411**, 581–583 (2001)
8. Fua, P.: A parallel stereo algorithm that produces dense depth maps and preserves image features. Machine Vision and Applications **6**(1), 35–49, December (1993)
9. Horridge, G.A.: Insects which turn and look. Endeavour N.S. **1**, 7–17 (1977)
10. Horridge, G.A.: The evolution of visual processing and the construction of seeing systems. Proceedings of the Royal Society of London. Series B **230**, 279–292 (1987)
11. Kirchner, W.H., Srinivasan, M.V.: Freely flying honeybees use image motion to estimate object distance. Naturwissenschaften **76**, 281–282 (1989)
12. Lehrer, M., Srinivasan, M.V., Zhang, S.W., Horridge, G.A.: Motion cues provide the bee's visual world with a third dimension. Nature (London) **332**, 356–357 (1988)
13. Neumann, T.R., Bülthoff, H.: Insect inspired visual control of translatory flight. In: Kelemen J, Sosik P (eds.) Proceedings of the ECAL 2001, pp. 627–636. Springer, Berlin (2001)
14. Ruffier, F., Franceschini, N.: Optic flow regulation: the key to aircraft automatic guidance. Robotics and Autonomous Systems **50**, 177–194 (2005)
15. Soccol, D., Thurrowgood, S., Srinivasan, M.V., A vision system for optic-flow-based guidance of UAVs. Proceedings, Ninth Australasian Conference on Robotics and Automation. Brisbane, 10–12 December (2007)
16. Srinivasan, M.V.: How insects infer range from visual motion. In: F.A. Miles, J. Wallman (eds.) Visual Motion and its Role in the Stabilization of Gaze. Elsevier, Amsterdam, pp. 139–156 (1993)
17. Srinivasan, M.V., Lehrer, M., Zhang, S.W., Horridge, G.A.: How honeybees measure their distance from objects of unknown size. Journal of Comparative Physiology A **165**, 605–613 (1989)
18. Srinivasan, M.V., Lehrer, M., Horridge, G.A.: Visual figure-ground discrimination in the honeybee: the role of motion parallax at boundaries. Proceedings of the Royal Society of London. Series B **238**, 331–350 (1990)
19. Srinivasan, M.V., Lehrer, M., Kirchner, W., Zhang, S.W.: Range perception through apparent image speed in freely-flying honeybees. Visual Neuroscience **6**, 519–535 (1991)

20. Srinivasan, M.V., Thurrowgood, S., Soccol, D.: An optical system for guidance of terrain following in UAVs. Proceedings, IEEE International Conference on Advanced Video and Signal Based Surveillance (AVSS '06), Sydney, 51–56 (2006)

21. Srinivasan, M.V., Zhang, S.W.: Visual control of honeybee flight. In: M. Lehrer (ed.) Orientation and Communication in Arthropods, pp. 67–93. Birkhäuser Verlag, Basel (1997)

22. Srinivasan, M.V., Zhang, S.W.: Visual navigation in flying insects. In: M. Lappe (ed.) International Review of Neurobiology, Vol. 44, Neuronal Processing of Optic Flow, pp. 67–92. Academic Press, San Diego (2000)

23. Srinivasan, M.V., Zhang, S.W., Altwein, M., Tautz, J.: Honeybee navigation: nature and calibration of the 'odometer'. Science **287**, 851–853 (2000)

24. Srinivasan, M.V., Zhang, S.W., Chahl, J.S., Barth, E., Venkatesh, S.: How honeybees make grazing landings on flat surfaces. Biological Cybernetics **83**, 171–183 (2000)

25. Srinivasan, M.V., Zhang, S.W., Chahl, J S, Stange, G, Garratt, M.: An overview of insect inspired guidance for application in ground and airborne platforms. Proceedings of the Institution of Mechanical Engineers. Part G, Journal of Aerospace Engineering **218**, 375–388 (2004)

26. Srinivasan, M.V., Zhang, S.W., Chandrashekara, K.: Evidence for two distinct movement-detecting mechanisms in insect vision. Naturwissenschaften **80**, 38–41 (1993)

27. Srinivasan, M.V., Zhang, S.W., Lehrer, M., Collett, T.S.: Honeybee navigation en route to the goal: visual flight control and odometry. The Journal of Experimental Biology **199**, 237–244 (1996)

28. Zufferey, J.C., Floreano, D.: Fly-inspired visual steering of an ultralight indoor aircraft. IEEE Transactions on Robotics **22**, 137–146 (2006)